APPLIED SCIENCES AND ENGINEERING

Microfluidic dielectrophoresis illuminates the relationship between microbial cell envelope polarizability and electrochemical activity

Qianru Wang[1], A.-Andrew D. Jones III[1]*, Jeffrey A. Gralnick[2], Liwei Lin[3], Cullen R. Buie[1†]

Electrons can be transported from microbes to external insoluble electron acceptors (e.g., metal oxides or electrodes in an electrochemical cell). This process is known as extracellular electron transfer (EET) and has received considerable attention due to its applications in environmental remediation and energy conversion. However, the paucity of rapid and noninvasive phenotyping techniques hinders a detailed understanding of microbial EET mechanisms. Most EET phenotyping techniques assess microorganisms based on their metabolism and growth in various conditions and/or performance in electrochemical systems, which requires large sample volumes and cumbersome experimentation. Here, we use microfluidic dielectrophoresis to show a strong correlation between bacterial EET and surface polarizability. We analyzed surface polarizabilities for wild-type strains and cytochrome-deletion mutants of two model EET microbes, *Geobacter sulfurreducens* and *Shewanella oneidensis*, and for *Escherichia coli* strains heterologously expressing *S. oneidensis* EET pathways in various growth conditions. Dielectrophoretic phenotyping is achieved with small cell culture volumes (~100 μl) in a short amount of time (1 to 2 min per strain). Our work demonstrates that cell polarizability is diminished in response to deletions of crucial outer-membrane cytochromes and enhanced due to additions of EET pathways. Results of this work hold exciting promise for rapid screening of direct EET or other cell envelope phenotypes using cell polarizability as a proxy, especially for microbes difficult to cultivate in laboratory conditions.

INTRODUCTION

Extracellular electron transfer (EET) (*1*, *2*) is the capacity for microbes to transfer electrons between their interior and external electron donors or acceptors during anaerobic respiration. It empowers cell growth and/or maintenance of exoelectrogens and electrotrophs and makes them versatile for multiple applications including environmental remediation (*2*), microbial fuel cells (MFCs) (*3*, *4*), and microbial electrosynthesis (*5*, *6*). Microbial EET mechanisms have been explored using a number of dissimilatory metal-reducing bacteria (DMRB), among which *Geobacter* and *Shewanella* are the most studied. For example, *Geobacter sulfurreducens* uses a network of multiheme cytochromes (*4*, *7*–*9*) to transfer electrons, while *Shewanella oneidensis* uses different sets of proteins, forming a metal-reducing (Mtr) pathway (*10*), to route electrons across the cell envelope. Moreover, *G. sulfurreducens* can form extracellular conductive pili (*11*), and *S. oneidensis* can produce outer-membrane and periplasmic extensions (*12*) that may enable long-distance electron transport. Extensive genetic and biochemical analysis has substantially enhanced our understanding of the EET pathway in a few well-established model microorganisms and hastened the improvement of their related biotechnological applications. However, key knowledge gaps still remain, partially due to the fact that phenotyping techniques for EET investigations lag behind the development of genotyping methods. Although at least 111 putative *c*-type cytochromes have been reported for *G. sulfurreducens* by complete genome sequencing (*13*), only a few have been fully understood in their phenotype-genotype relationships and physiological functions (*7*, *8*). Conventional phenotyping techniques to evaluate microbial EET, including cell growth in various conditions (*8*), measurement of redox products [e.g., Fe(II) and Mn(III) concentrations] (*8*, *9*, *14*, *15*), and power output in MFCs (*4*, *16*–*18*), are time consuming and require large sample volumes, impeding the investigation of difficult-to-culture or slow-growing microorganisms. Rapid and precise phenotyping strategies for microbial EET are imperative to uncover the phenotype-genotype relationship and to select superior candidates for optimized production in microbial electrochemical systems. Recently, the electrical conductivity of individual *G. sulfurreducens* pili (*19*) and electrode-grown biofilms (*20*, *21*) have been measured, where *G. sulfurreducens* components/networks were treated as electronic materials. Compared to traditional biochemical analysis, these electrical phenotyping methods provide important parameters for *G. sulfurreducens* EET modeling and suggest the possibility to quantify EET using intrinsic physical properties of microbes.

The advancement of microfluidic systems facilitates investigation of cellular electrical properties (*22*–*24*), opening a new dimension for understanding complex physiological cellular states. Microfluidic systems using dielectrophoresis (DEP) (*25*) induced by DC electric fields enable the study of cell surface properties exclusively (see section S1) (*24*, *26*–*29*), unlike cell impedance measurements (*22*) and electrorotation techniques (*23*) that use high-frequency electric fields to detect cell internal properties. Previous work has shown that three-dimensional insulator-based DEP (3DiDEP) provides a high-sensitivity approach to probe bacterial envelope phenotypes with subspecies-level resolution (*27*, *28*). In this work, we demonstrate that microbial EET (a cellular physiological property) is correlated with cell surface polarizability (an electrical property) that can be easily measured by microfluidic systems using 3DiDEP (Fig. 1, A to C). This work is the first to show the strong correlation between bacterial EET and cell

[1]Department of Mechanical Engineering, Massachusetts Institute of Technology, 77 Massachusetts Avenue, Cambridge, MA 02139, USA. [2]Department of Plant and Microbial Biology, BioTechnology Institute, University of Minnesota Twin Cities, 1479 Gortner Avenue, St. Paul, MN 55108, USA. [3]Department of Mechanical Engineering, University of California, Berkeley, 1113 Etcheverry Hall #1740, Berkeley, CA 94720-1740, USA.
*Present address: Department of Chemical Engineering and Department of Mechanical and Industrial Engineering, Northeastern University, 360 Huntington Avenue, Boston, MA 02115, USA.
†Corresponding author. Email: crb@mit.edu

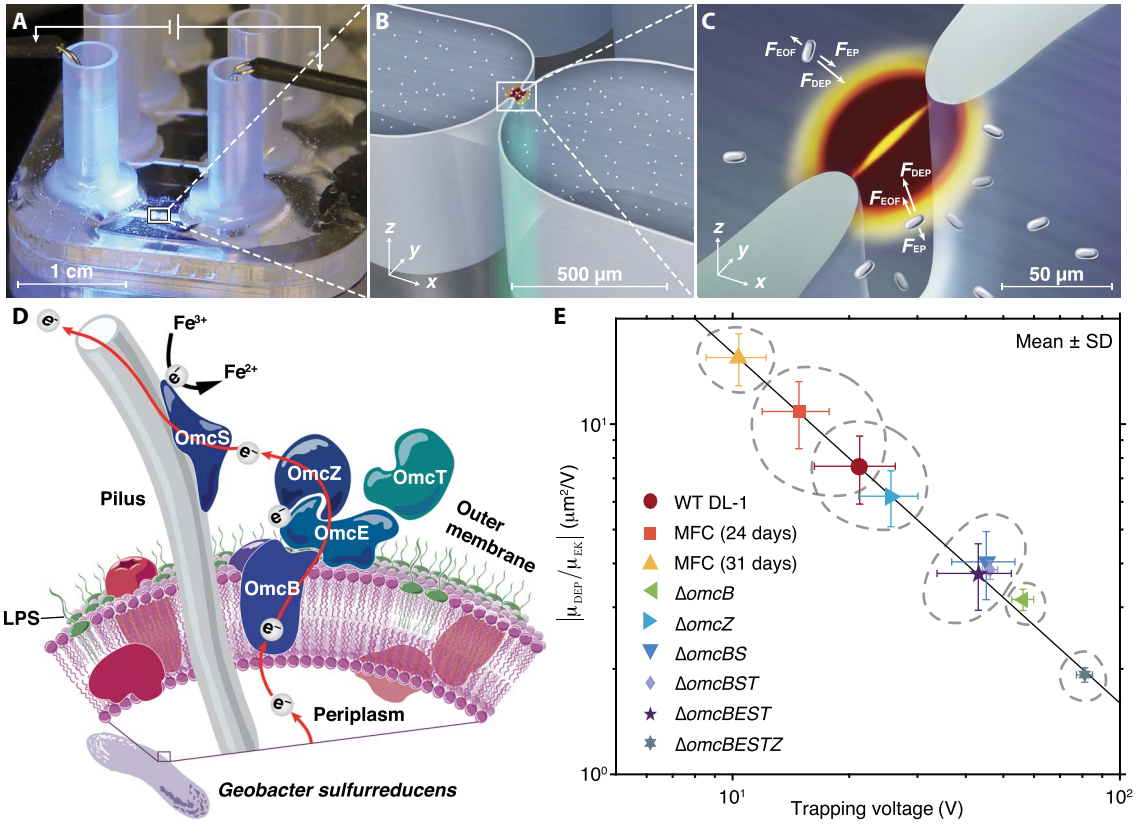

Fig. 1. DEP phenotyping of *G. sulfurreducens*. (**A**) 3DiDEP microfluidic device with an array of multiple microchannels. A DC potential difference increasing linearly with time at 1 V/s was applied across the channel. Credit: Qianru Wang, MIT. (**B**) Magnified view of the microchannel highlighting the constricted area. (**C**) Schematic depicting the 3DiDEP trapping principle. Bacteria near the constriction are immobilized when the DEP force ($\vec{F}_{DEP}$), which is proportional to $\nabla\vec{E}^2$, is balanced by drag forces due to the background electroosmotic flow ($\vec{F}_{EOF}$) and electrophoresis ($\vec{F}_{EP}$). The magnitude distribution of the *x* component of $\nabla\vec{E}^2$ is illustrated in the background color scale (dark red indicates higher values). (**D**) Schematic showing that *G. sulfurreducens c*-type outer-membrane cytochromes mediate EET. (**E**) Measured trapping voltage [the threshold applied voltage at the onset of 3DiDEP trapping depicted in (C)] was plotted against the ratio of DEP mobility (μ_{DEP}) to the magnitude of linear electrokinetic mobility (μ_{EK}) of WT *G. sulfurreducens* DL-1, DL-1 inoculated in an MFC anode for 24 and 31 days, and various indicated cytochrome-deletion mutants. A significant difference ($P < 0.05$) was found between data groups isolated by dashed circles using a Kruskal-Wallis test. The black line indicates the inverse relationship between the ratio $|\mu_{DEP}/\mu_{EK}|$ and the applied voltage.

surface polarizability. Polarizability represents the tendency to form electric dipoles in a material (not necessarily charged) subjected to externally applied electric fields. Cell surface polarizability represents the overall dielectric properties at the cell/medium interface. It should be noted that we consider polarizability as a physical property adopted from the area of electromagnetics, rather than the biological concept (e.g., cell polarity) defined as the ability to form asymmetric organization of cellular components and shape as in the case of cell division and cell migration. We show that *c*-type outer-membrane cytochromes known to be responsible for EET in the microbial cell envelope contribute to the cell surface polarizability. The compositional diversity of the cell envelope induced by the presence/abundance of *c*-type cytochromes significantly affects cell surface polarizability. Our analysis of wild-type (WT) *G. sulfurreducens* DL-1 and various cytochrome-deletion mutants shows that deficiency in expressing *c*-type outer-membrane cytochromes essential for EET measurably decreases cell surface polarizability. Similar correlations were found with *S. oneidensis* and *Escherichia coli* heterologously expressing *S. oneidensis* EET pathways. Moreover, we show that the decrease of *S. oneidensis* polarizability due to loss of EET pathways can be recovered by reintroducing the EET pathway. In addition, activation of the microbial EET pathway by switching electron acceptors from pure fumarate to an MFC anode (for *G. sulfurreducens* DL-1) or Fe(III) citrate (for *S. oneidensis* strains) enhances cell surface polarizability.

RESULTS

Assessment of cell surface polarizability using DEP

Cell surface polarizability was quantified by the Clausius-Mossotti factor (κ_{CM}), a measure of the relative polarizability of the cell compared to the surrounding medium. We used microfluidic 3DiDEP devices employing linear sweep analysis (*28*), in which the applied electric field increases linearly with time across the microchannel (Fig. 1A). The microchannel contains a 3D insulating constriction with a cross-sectional area 100 times smaller than that of the main channel, creating a strong electric field gradient in the vicinity of the constriction (Fig. 1B). In this study, Brownian motion and cell motility effects are small compared to DEP. Bacteria are driven toward the microchannel constriction by the combination of two linear electrokinetic (EK) effects, electroosmosis and electrophoresis. The resulting electrokinetic velocity is proportional to the applied electric field ($\vec{E}$) as

$$\vec{u}_{EK} = \mu_{EK}\vec{E} \quad (1)$$

where μ_{EK} is the combined linear electrokinetic mobility (*30*). Cells of the three bacterial species investigated are rod shaped and can be modeled as ellipsoidal particles with semi-axes $a > b = c$ (*31*). Because both shear and electro-orientation tend to align the prolate cell in the direction of flow (i.e., the electric field direction) (*32*, *33*), the Stokes' drag is estimated as

$$\vec{F}_{Drag} = 6\pi\xi\eta a\vec{u} \quad (2)$$

where η is the viscosity of the surrounding medium and the Perrin friction factor (*34*) is

$$\xi = \sqrt{1-p^2}/\ln[(1+\sqrt{1-p^2})/p] \quad (3)$$

with $p = b/a$. Near this constricted region, the DEP force exerted on a bacterium by a DC electric field can be expressed as (*35*)

$$\vec{F}_{DEP} = 2\pi a b^2 \varepsilon_m \kappa_{CM} \nabla\vec{E}^2 \quad (4)$$

where ε_m is the permittivity of the surrounding medium. The induced DEP velocity is

$$\vec{u}_{DEP} = \frac{\vec{F}_{DEP}}{6\pi\xi\eta a} = \mu_{DEP}\nabla\vec{E}^2 \quad (5)$$

where the DEP mobility, μ_{DEP}, is specified as

$$\mu_{DEP} = \frac{b^2\varepsilon_m\kappa_{CM}}{3\eta\xi} \quad (6)$$

Bacteria are immobilized when DEP balances bacterial motion due to linear electrokinetic effects (Fig. 1C). Given Eqs. 1 and 5, the criterion for 3DiDEP immobilization of a single cell is (*27*, *30*, *36*)

$$\mu_{EK}\vec{E}\cdot\vec{E} + \mu_{DEP}(\nabla\vec{E}^2)\cdot\vec{E} = 0 \quad (7)$$

On the basis of Eqs. 6 and 7, the Clausius-Mossotti factor (κ_{CM}) can be estimated from the experimentally determined minimum potential ("trapping voltage") required for 3DiDEP immobilization at the microchannel constriction.

Correlating *G. sulfurreducens* polarizability with electrochemical activity

A set of proteins, particularly *c*-type outer-membrane cytochromes localized on the cell surface (Fig. 1D), are known to regulate the electron flow across the cell envelope of *G. sulfurreducens* (*7*–*9*, *17*). To quantify a possible correlation between *G. sulfurreducens* electrochemical activity and cell surface polarizability, DL-1 and various cytochrome-deletion mutants (*8*, *16*, *37*) were grown with the soluble electron acceptor fumarate and were then evaluated using the 3DiDEP device. Fumarate was selected as the electron acceptor because the OmcB-deficient strains grow as well as the WT strain when reducing fumarate, but their growth is diminished with Fe(III) citrate and is not sustainable when reducing Fe(III) oxide (*8*). Fumarate-grown *G. sulfurreducens* DL-1 has been confirmed to express outer-membrane cytochromes OmcB, OmcE, OmcS, OmcT, and OmcZ by several previous studies (*7*–*9*, *15*, *16*). In addition, we compare cell surface polarizability of fumarate-grown DL-1 and DL-1 harvested from an MFC anode with varying incubation times to examine whether 3DiDEP is sensitive enough to detect cell surface phenotypic changes induced by alteration of growth conditions. Two MFC strains were measured, one of which was directly inoculated from the fumarate-grown DL-1 and thus required long-term MFC incubation to adapt to the transition of reducing soluble/insoluble electron acceptors. As a further proof of the possible correlation between cell polarizability and MFC inoculation, we analyzed another better adapted MFC strain, which was inoculated from DL-1 kept with the insoluble electron acceptor, Fe(III) oxide. Strains used in this study are summarized in Table 1.

The trapping voltages for the onset of 3DiDEP immobilization (the *x*-axis data in Fig. 1E; see movie S1) were measured for the strains and used to determine the local critical electric field ($\vec{E}$) by numerical simulation. The numerically estimated electric field leads to the ratio between the magnitudes of DEP mobility versus linear electrokinetic mobility (the *y*-axis data in Fig. 1E), $|\mu_{DEP}/\mu_{EK}|$, which is inversely proportional to the trapping voltage. The trapping voltage measured for the fumarate-grown DL-1 is significantly distinguished ($P < 0.05$) from that of the fumarate-grown mutants deficient in expressing the outer-membrane cytochrome OmcB and the DL-1 strain grown in an MFC for 31 days. Because the trapping voltage is a function of three parameters (Eqs. 6 and 7), including the cell polarizability (κ_{CM}), linear electrokinetic mobility (μ_{EK}), and cell morphology (b and ξ), we measured linear electrokinetic mobility and cell dimensions separately to decouple their effects. Linear electrokinetic mobilities (Fig. 2A) were obtained by tracking cell trajectories in straight microfluidic channels under DC electric fields using particle image velocimetry (movie S2) (*38*). Removing outer-membrane cytochromes and MFC inoculation did not induce significant differences in measured linear electrokinetic mobilities (Fig. 2A), suggesting small variations of zeta potentials (or surface charge conditions) at the cell/medium interface, given that the electrophoretic mobility scales with zeta potential (ζ) as $\mu_{EP} \sim (\varepsilon_m\zeta)/\eta$. One hypothesis is that surface charges can be conferred by other cell components including the lipopolysaccharide (LPS), which is more abundant on the cell surface compared to outer-membrane cytochromes. Another explanation posits that *G. sulfurreducens* is able to express and use alternative cytochromes when some are unavailable, which may compensate for the variations in cell surface charges. DEP mobilities of these strains (Fig. 2B), μ_{DEP}, were derived from the ratio μ_{DEP}/μ_{EK} and measured linear electrokinetic mobilities according to Eq. 7. Compared to cell surface polarizability, DEP mobility captures both cellular surface dielectric properties and cell shape information. Although the genetic changes made to the cell envelope and the change in growth conditions can lead to some discrepancies in cell major and minor semi-axis (Fig. 2, C and D), these variations have no significant influence on *G. sulfurreducens* polarizability. Cell morphology can affect the cell motion by (i) altering the drag force via the Perrin friction factor, ξ (Eq. 2), and (ii) changing the DEP force, which depends on the short semi-axis, b (Eq. 4). The ratio ξ/b^2 (Fig. 2E) indicates how much the ellipsoidal cell shape influences the drag force versus the DEP force. Because the DEP mobility for a spherical particle with a radius r is given by $\mu_{DEP-sphere} = \frac{r^2\varepsilon_m\kappa_{CM}}{3\eta}$,

Table 1. Strains used in this work.

Strain	Relative genotype	Source
G. sulfurreducens strains		
WT DL-1	*G. sulfurreducens* strain DL-1, WT	Leang *et al.* (*8*)
Δ*omcB*	WT DL-1 strain without *omcB*	Leang *et al.* (*8*)
Δ*omcZ*	WT DL-1 strain without *omcZ*	Nevin *et al.* (*16*)
Δ*omcBS*	WT DL-1 strain without *omcB/omcS*	Leang *et al.* (*8*)
Δ*omcBST*	WT DL-1 strain without *omcB/omcS/omcT*	Leang *et al.* (*8*)
Δ*omcBEST*	WT DL-1 strain without *omcB/omcE/omcS/omcT*	Voordeckers *et al.* (*37*)
Δ*omcBESTZ*	WT DL-1 strain without *omcB/omcE/omcS/omcT/omcZ*	Voordeckers *et al.* (*37*)
S. oneidensis strains		
WT MR-1	*S. oneidensis* strain MR-1, WT	Coursolle and Gralnick (*10*)
ΔMtr	Δ*mtrB*/Δ*mtrE*/Δ*mtrC*/Δ*omcA*/Δ*mtrF*/Δ*mtrA*/Δ*mtrD*/Δ*dmsE*/Δ*SO4360*/Δ*cctA*/Δ*recA*	Coursolle and Gralnick (*10*)
ΔMtr+MtrABC	ΔMtr strain carrying plasmid *pmtrB/mtrC/mtrA*	Coursolle and Gralnick (*10*)
ΔMtr+MtrDEF	ΔMtr strain carrying plasmid *pmtrE/mtrF/mtrD*	Coursolle and Gralnick (*10*)
ΔMtr+vector	ΔMtr strain carrying an empty vector pBBR-BB	Coursolle and Gralnick (*10*)
E. coli strains		
ccm	*E. coli* strain C43 carrying *ccmA-H*	Jensen *et al.* (*42*)
ccm+CymA/MtrABC	Strain ccm cotransformed with *cymAmtrCAB*	Jensen *et al.* (*42*)

physically (with Eq. 6) $\frac{b}{\sqrt{\xi}}$ can be considered as the equivalent DEP radius for an ellipsoidal particle. No significant difference was found for the ratio ξ/b^2 among the investigated *G. sulfurreducens* strains (Fig. 2E), and thus, their DEP mobility (Fig. 2B) and Clausius-Mossotti factor (Fig. 2F) follow a similar trend. The Clausius-Mossotti factors represent the surface polarizabilities of the *G. sulfurreducens* strains and were estimated according to Eq. 6. Many authors report Clausius-Mossotti factor being restricted from −0.5 to 1, but this is done assuming homogeneous spherical particles. However, the Clausius-Mossotti factor of bacteria can be higher than 1 (fig. S1) due to multiple physiological features such as their nonspherical shapes (*29*) and/or charged soft extracellular layers (*39*), for example, LPS and pili produced by *G. sulfurreducens* (see section S1 for detailed explanation).

As shown in Fig. 2F, removing *c*-type outer-membrane cytochromes can lead to decreased cell surface polarizability in *G. sulfurreducens*. The Δ*omcBESTZ* quintuple mutant displayed a 70% decrease in cell surface polarizability compared to strain DL-1. Moreover, removing different genes encoding outer-membrane cytochromes results in distinct effects on *G. sulfurreducens* surface polarizability. As shown in Fig. 2F, all the mutants missing gene *omcB* (Δ*omcB*, Δ*omcBS*, Δ*omcBST*, Δ*omcBEST*, and Δ*omcBESTZ*) show significantly suppressed polarizability ($P < 0.02$) compared to strain DL-1. Removing OmcB alone induces a decrease in cell surface polarizability by a factor of 2 (Δ*omcB* versus DL-1 in Fig. 2F), suggesting a substantial impact of OmcB on *G. sulfurreducens* surface polarizability. However, removing OmcZ alone did not change cell polarizability significantly (Δ*omcZ* versus DL-1 in Fig. 2F), while simultaneous deletion of OmcBESTZ induces a further decrease in cell surface polarizability compared to the quadruple mutant Δ*omcBEST* (Δ*omcBEST* versus Δ*omcBESTZ* in Fig. 2F). We hypothesize that one reason for this discrepancy is that OmcZ has a smaller impact on surface polarizability than OmcB, which could be due to their distinct locations within the cell envelope. OmcB is embedded in the outer membrane of *G. sulfurreducens* and partially exposed to the outer surface (*15*), while OmcZ is only loosely bound to the outer membrane (Fig. 1A) (*7*, *16*, *17*). Another possible reason is that the single-deletion mutant Δ*omcZ* is adapted by up-regulating other outer-membrane cytochromes (table S1) (*17*), which may mask any potential drop in cell surface polarizability. This adaptation capability of *G. sulfurreducens* may also explain the fact that there is no significant difference in cell surface polarizability among the mutants Δ*omcB*, Δ*omcBS*, Δ*omcBST*, and Δ*omcBEST*. Otherwise, it is possible that the presence of OmcE, OmcS, and OmcT does not have a large effect on *G. sulfurreducens* surface polarizability. *G. sulfurreducens* uses different outer-membrane cytochromes for EET when reducing different kinds of electron acceptors (*7*–*9*, *14*–*17*). For instance, removing OmcB results in significant deficiency for *G. sulfurreducens* to reduce both soluble and insoluble Fe(III) (*8*, *14*, *15*), while OmcZ is only essential when an MFC anode serves as the electron acceptor (*7*, *16*, *17*). Despite the adaptation capacity of *G. sulfurreducens*, a number of outer-membrane cytochromes (including OmcB and OmcZ) are not interchangeable in their physiological functions for EET (*14*). For example, OmcB-deficient mutants never adapt to grow with Fe(III) oxide (*14*), while OmcZ-deficient mutants show severe inhibition in MFC current production with no long-term adaptation (*17*). Our observation of distinct cell polarizability between OmcB- and OmcZ-deficient mutants indicates the potential of using microfluidic DEP to separate *G. sulfurreducens* based on its activity for reducing different electron acceptors. The physiological roles of the *c*-type outer-membrane cytochromes investigated in this work have been well studied for various growth conditions and are summarized in table S1.

The MFC strains (in Fig. 2F) were directly inoculated from the fumarate-grown DL-1 cultures and grown in an "H-cell," with the two graphite electrodes connected by a titanium wire through a 1-kilohm resistor. It has been reported that *G. sulfurreducens* adapted in anode-respiring conditions has substantially enhanced EET compared to the inoculum due to up-regulation of a number of *c*-type outer-membrane cytochromes (*16*, *17*) and pili (table S1) (*16*). Correspondingly, we observed that the cell surface polarizability for strain DL-1 is doubled compared to that of its inoculum after growing in an MFC for 31 days. Moreover, comparing strains DL-1, MFC (24 days), and MFC (31 days) suggests an increasing trend in cell surface polarizability as MFC incubation time increases (Fig. 2F). Fumarate-grown DL-1 is not immediately capable of significant current production (*16*), and cells gradually (in roughly 3 weeks) adapt to anode respiration over time. Our 24- and 31-day MFC strains achieved a current density of 0.046 and 0.404 A/m^2 and a power density of 0.016 and 0.246 W/m^2, respectively, suggesting different production in related outer-membrane cytochromes and pili. We hypothesize that phenotypic changes in the expression

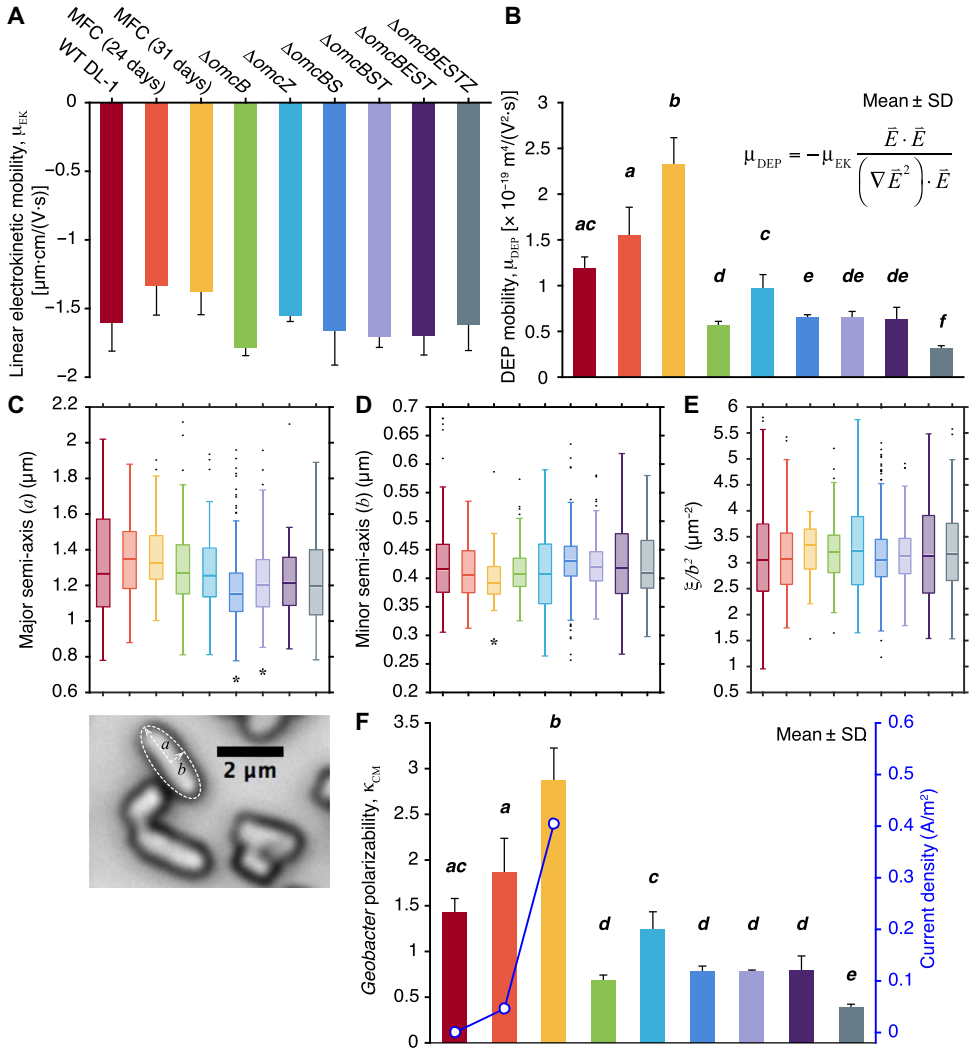

Fig. 2. *G. sulfurreducens* cell polarizability is positively correlated with EET capacity. (**A**) Linear electrokinetic mobility (mean ± SD), μ_{EK}, of the studied nine strains of *G. sulfurreducens*. (**B**) DEP mobility, μ_{DEP}, of the studied nine strains of *G. sulfurreducens*. Pairwise comparison using two-sample *t* test (two-tailed) shows significant difference ($P < 0.03$) between groups not sharing letters (italic bold). (**C** to **E**) Box-whisker plots of cell major semi-axis (C), minor semi-axis (D), and the ratio of Perrin friction factor to the square of cell short semi-axis ξ/b^2 (E) by ellipsoidal fit for the nine investigated *G. sulfurreducens* strains indicate median and interquartile ranges (IQRs). The whiskers extend to 1.5 IQR below the 25th percentile and above the 75th percentile, respectively. Blank dots indicate the outliers. Asterisks indicate significant difference ($P < 0.01$) compared to the control (WT DL-1) by a Kruskal-Wallis test. The numbers of measured cells (*n*) are 150, 100, 100, 244, 100, 445, 238, 50, and 100, respectively, following the order in (A). Inserted plot is a high-magnification micrograph showing the ellipsoidal fit of a WT DL-1 bacterium. (**F**) *G. sulfurreducens* polarizability, represented by the Clausius-Mossotti factor (κ_{CM}), of the nine investigated strains (left *y* axis), as well as the current density (blue circles, right *y* axis) generated by *G. sulfurreducens* grown in an MFC. Italic bold letters above the bars show the result of pairwise comparison using two-sample *t* test (two-tailed) with the following number of repeats: $n = 3$ (WT DL-1, Δ*omcBST*), $n = 4$ (Δ*omcB*, Δ*omcZ*, Δ*omcBS*, Δ*omcBEST*, and Δ*omcBESTZ*), $n = 5$ (MFC, 24 days), and $n = 7$ (MFC, 31 days). A significant difference ($P < 0.02$) was found between groups not sharing letters. Colors in all panels correspond to the legend in Fig. 1E.

of outer-membrane cytochromes and pili after long-term MFC incubation contribute to stronger cell surface polarizability, resulting in the positive correlation between cell polarizability and MFC incubation time. Data for strains with an MFC incubation time shorter than 24 days are not provided because the cell concentration was too low [OD_{600} (optical density at 600 nm) < 0.05 measured after sample preparation] for DEP-based screening. The MFC strains (in Fig. 2F) show a growth rate slower than some of the reported values, given that their inoculum—the fumarate-grown DL-1—is not immediately adapted to reduce the MFC anode. In addition, we used an anode surface area and MFC configuration different from the conditions in previous studies, which may also explain the difference in growth rate. To address this problem, we also analyzed another anode-respiring DL-1 strain following the protocol by Bond and Lovley (*4*). To obtain this new MFC strain, DL-1 cells were maintained in medium with Fe(III) oxide to be better adapted to reduce insoluble electron acceptors. Fe(III) oxide particles in the cell cultures were then eliminated by transferring the cells three times in medium containing 40 mM fumarate before inoculation into the MFC (see Materials and Methods for further details). The new MFC strain shows a faster growth rate and demonstrates once again that *G. sulfurreducens* surface polarizability increases with incubation time in the MFC (fig. S2).

This indicates that cell surface polarizability is sensitive enough to detect the phenotypic change of *G. sulfurreducens* during growth in an MFC and further proves that *G. sulfurreducens* EET correlates with cell surface polarizability. It should be noted that anode-grown *G. sulfurreducens* biofilms consist of cells with heterogeneous physiological properties. Our 3DiDEP technique captures the most polarizable cells within a heterogeneous population and thus does not capture the distributions of cell polarizability values. Further analysis at the single-cell level or separate 3DiDEP measurements of cells within the biofilm but taken from different distances away from the electrode surface are areas for possible future work. A number of studies show that *G. sulfurreducens* can adapt to electrode respiration over time for enhanced efficiency in current production on a per cell basis (*7*, *16*–*18*). In addition, cyclic voltammetry of anode-respiring *G. sulfurreducens* has shown that the maximum biofilm thickness and current production are predominantly limited by cell EET rather than the mass transport of reactants (*40*). This suggests opportunities for evolutionary selection of *G. sulfurreducens* (and other electrochemically active microorganisms) for optimal current production using cell surface polarizability as a proxy.

S. oneidensis polarizability is positively correlated with EET

To explore if the correlation between cell surface polarizability and microbial EET is generalizable to other electrochemically active microorganisms and other growth conditions, we investigated *S. oneidensis*, a facultative anaerobe that uses a different EET pathway than *G. sulfurreducens*. EET in *S. oneidensis* requires the Mtr respiratory pathway, which consists of a periplasmic *c*-type cytochrome (e.g., MtrA or MtrD), an integral β-barrel protein located in the outer-membrane (e.g., MtrB or MtrE), and an outer-membrane decaheme *c*-type cytochrome (e.g., MtrC, MtrF, or OmcA) (*10*, *41*). These components cooperatively facilitate electron transfer from the periplasm of the cell to the extracellular electron acceptors (Fig. 3A). Because these Mtr components show various activities in iron reduction, we analyzed five *S. oneidensis* strains (Table 1) to address the following three questions: (i) Is the correlation between cell polarizability and EET generalizable to *Shewanella* strains? (ii) Is dielectrophoretic screening sufficiently sensitive to distinguish the alterations made in different Mtr pathways? (iii) Is this correlation affected by change of growth conditions? The five strains investigated here are the WT strain MR-1, a *S. oneidensis* strain deficient in iron reduction by knocking out all genes identified in the

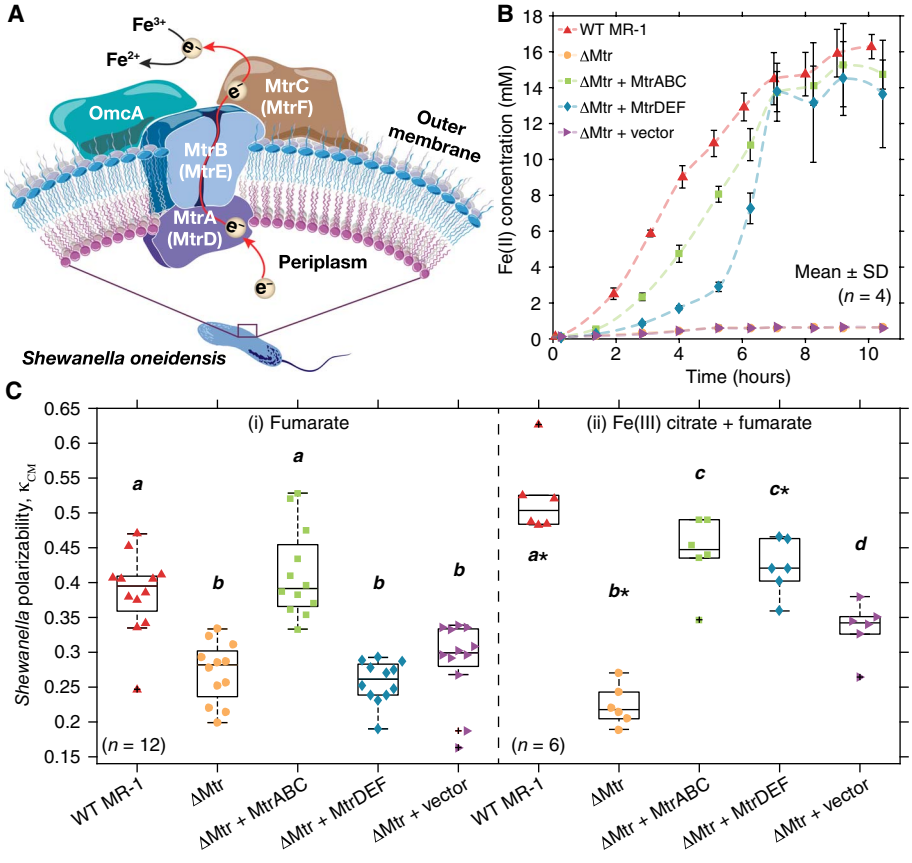

Fig. 3. DEP screening indicates positive correlation between *S. oneidensis* polarizability and EET activity. (**A**) Schematic of the Mtr EET pathway in the *S. oneidensis* cell envelope. (**B**) Fe(III) citrate reduction over time measured for *S. oneidensis* WT strain MR-1, strain deficient in expressing both MtrABC and MtrDEF EET conduits (ΔMtr), and ΔMtr complemented with indicated proteins. Error bars indicate the SD. (**C**) Polarizability of the five *S. oneidensis* strains corresponding to (B) grown with different electron accepters, namely, (i) 60 mM pure fumarate and (ii) 15 mM Fe(III) citrate supplemented with a small amount (10 mM) of fumarate. Growth conditions in (B) and (C) (ii) are identical. The box-whisker plots indicate median and IQRs, with whiskers extending to 1.5 IQR below the 25th percentile and above the 75th percentile, respectively. Black crosses indicate outliers. Multiple comparison test of group means using one-way analysis of variance (ANOVA) suggests a significant difference ($P < 0.05$) between groups labeled with different letters. Asterisk indicates a significant difference ($P < 0.03$, two-tailed *t* test) between the polarizability of iron-reducing *S. oneidensis* (ii) and that of its fumarate-reducing counterpart (i).

Mtr pathway (ΔMtr), and three complemented strains including various combinations of Mtr components, namely, the ΔMtr strain complemented with *mtrABC*, *mtrDEF*, and the empty vector pBBR-BB (*10*). We measured the iron reduction rate of the five strains grown with both Fe(III) citrate and a small amount of fumarate (to ensure the growth of all strains). As expected, the ΔMtr strain and the strain with the empty vector are defective in Fe(III) citrate reduction (Fig. 3B). MR-1 has the highest iron reduction rate, followed by the complemented strain expressing *mtrABC*, which shows roughly twice the reduction rate compared to that of the complemented strain expressing *mtrDEF* (Fig. 3B). Our results suggest that the *mtrABC* paralog is superior to *mtrDEF* in terms of Fe(III) citrate reduction, agreeing with previous observations (*10*). We then performed dielectrophoretic screening with these five *S. oneidensis* strains grown in two conditions: 10 mM lactate (electron donor) and 60 mM fumarate (electron acceptor), and 20 mM lactate and 15 mM Fe(III) citrate supplemented with 10 mM fumarate (corresponding to the growth condition in Fig. 3B). In both circumstances, deletion of Mtr pathways lowered *S. oneidensis* polarizability (ΔMtr versus MR-1 in Fig. 3C), and this change is reversible by adding EET conduits, demonstrating a strong correlation between cell polarizability and EET in *S. oneidensis*. The corresponding data for the linear electrokinetic mobility and cell morphology can be found in fig. S3. When reducing fumarate, the drop of *S. oneidensis* polarizability is recovered by adding the MtrABC EET conduit as opposed to the MtrDEF EET conduit (Fig. 3C, i), suggesting that the level of *S. oneidensis* polarizability can (at least partially) be attributed to the presence of MtrABC. Fumarate respiration in *S. oneidensis* occurs only in the periplasm of the cell, that is, the outer-membrane components in the Mtr pathway are not involved in condition (i). However, all metal reduction occurs extracellularly (*10*). Thus, in the second condition, all the EET components in the Mtr pathway are involved to reduce Fe(III) citrate. Cell surface polarizabilities measured for the MR-1 and complemented strain expressing *mtrDEF* (Fig. 3C, ii) are both significantly greater than cell surface polarizabilities measured for their fumarate-reducing counterparts (Fig. 3C, i), while no statistical difference was observed between the strains complemented with *mtrABC* grown in the two conditions. In addition, the ΔMtr strain complemented with *mtrDEF* shows a significantly stronger polarizability than the mutants ΔMtr and ΔMtr + vector. This comparison suggests that the outer-membrane component in the MtrDEF pathway starts to be involved in the EET process under conditions of excess iron, and the activation of the entire MtrDEF pathway can also enhance *S. oneidensis* cell surface polarizability. Comparing the five *S. oneidensis* strains grown with Fe(III) citrate suggests a ranking of cell polarizability ($P < 0.05$) (Fig. 3C, ii), approximately agreeing with the ranking of their iron reduction rate (Fig. 3B).

Introducing *S. oneidensis* EET conduits into *E. coli* enhances its cell surface polarizability

We further investigated the cell polarizability of *E. coli* heterologously expressing an Mtr respiratory pathway from *S. oneidensis*. Heterologous expression of CymA and MtrABC (localization as depicted in Fig. 3A) has been achieved by cotransforming the plasmid *cymAmtrCAB* with the cytochrome c maturation (*ccm*) plasmid into *E. coli* strain C43, enabling EET in *E. coli* (*42*). CymA is the *c*-type cytochrome anchored in the cytoplasmic membrane that donates electrons to a variety of respiratory pathways spanning the periplasm and outer membrane of *S. oneidensis* (*10*, *42*). Both the electrogenic *E. coli* strain expressing the MtrABC pathway (ccm + CymA/MtrABC) and the control strain (ccm) were grown with Fe(III) citrate and a small amount of fumarate. Previous studies have confirmed the expression and redox activity of CymA, MtrA, and MtrC in the electrogenic *E. coli* strain (*42*). Our dielectrophoretic screening shows that the electrogenic *E. coli* strain has a significantly stronger surface polarizability ($P < 0.0001$) compared to the ccm strain (Fig. 4A). This result provides further evidence that the presence of the MtrABC pathway enhances cell surface polarizability, regardless of the species of the microbe. The corresponding data for the linear electrokinetic mobility and cell morphology can be found in fig. S4. The electrogenic *E. coli* strain reduces Fe(III) citrate ~3.5× faster than the ccm strain (Fig. 4B), consistent with the results of previous studies (*42*), suggesting a positive correlation between iron reduction and cell surface polarizability. Figure 4C plots the cell surface polarizability of the five *S. oneidensis* strains and two *E. coli* strains grown with Fe(III) citrate against their iron reduction rates. It suggests that *S. oneidensis* has a superior iron reduction activity and cell polarizability compared to the electrogenic *E. coli*. It also suggests that 3DiDEP can be used to distinguish microbes from different species based on their iron reduction activity (or other phenotypes related to redox activity), although species may differ in their baseline cell polarizability.

DISCUSSION

This work represents the first demonstration of the correlation between EET and cell surface polarizability. By comparing the Clausius-Mossotti factor (κ_{CM}) of *G. sulfurreducens*, *S. oneidensis*, and electrogenic *E. coli* strains in different growth conditions, we show that microbial EET can be distinguished by cell surface polarizability using 3DiDEP, and the correlation is generalizable to multiple species. The level of cell surface polarizability is contingent on the amount of crucial outer-membrane cytochromes and the integrity of EET pathways, for example, high polarizability was found in both WT *G. sulfurreducens* and *S. oneidensis* (versus their cytochrome-deletion mutants) and *E. coli* expressing an Mtr respiratory pathway (versus the nonelectrogenic *E. coli* strain). The necessity of this correlation is further evidenced by the fact that the decrease in polarizability of MtrABC-deficient *S. oneidensis* can be complemented by providing a complete EET pathway in *trans*. In addition to removing or replacing EET components, increasing their redox activity by switching the growth conditions [e.g., respiration on an MFC anode or Fe(III) citrate versus fumarate] boosts cell surface polarizability. Moreover, EET components bearing different physiological functions (e.g., OmcB versus OmcZ in *G. sulfurreducens* and MtrABC versus MtrDEF in *S. oneidensis*) lead to diverse effects on cell surface polarizability.

This study introduces surface polarizability as a novel physical property for assessing EET in several types of Gram-negative bacteria. We show that surface polarizability can be measured using 3DiDEP noninvasively with low sample volume (~100 μl), which suggests exciting potential for phenotypic-based screening of electrochemically active organisms using microfluidic DEP. In addition, our results prompt a new question on how cell surface polarizability maps to electrochemical activity of Gram-positive or other bacteria that may use different EET mechanisms. Recent studies have revealed EET mechanisms distinct from the heme-based EET system in Gram-positive bacteria—they employ membrane-anchored lipoproteins (e.g., PplA), which recruit environmental flavins to "shuttle" electrons to extracellular acceptors (*43*). Genes for these newly identified proteins are present in diverse bacterial species spanning the Firmicutes phylum, including species in human microbiota and bacteria used for food fermentation or probiotics (*43*). Further investigations on the coupling between cell surface polarizability and flavin-based EET found in Gram-positive bacteria may potentiate a broader application for this approach. Moreover, compared

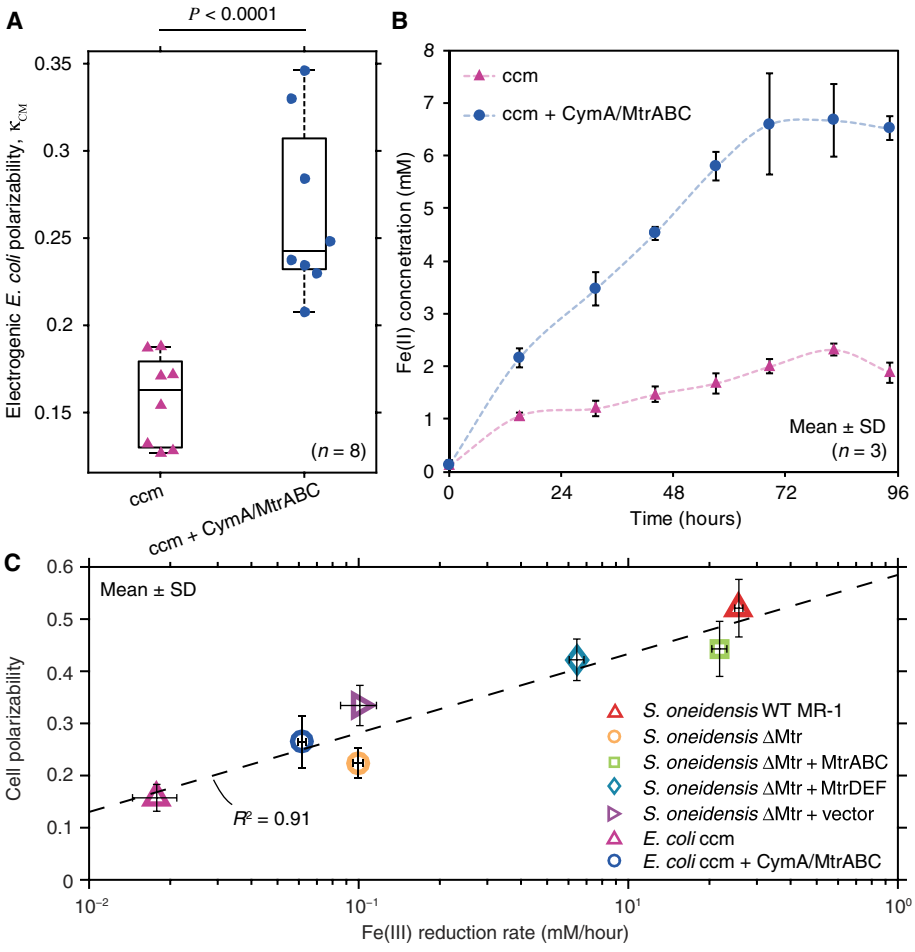

Fig. 4. *E. coli* introduced with EET pathways from *S. oneidensis* gains strong polarizability. (**A**) Polarizability of the *E. coli* strain transformed with an empty cytochrome c maturation (*ccm*) plasmid (control) and the strain cotransformed with *S. oneidensis* MtrABC EET conduit grown with 15 mM Fe(III) citrate and 10 mM fumarate. The electrogenic *E. coli* strain obtains significantly enhanced polarizability ($P < 0.0001$, two-tailed *t* test; $n = 8$) compared to the control. (**B**) Fe(III) citrate reduction over time measured for the control and the electrogenic *E. coli* strain. (**C**) Positive relationship between bacterial polarizability and iron reduction rate of the studied five *S. oneidensis* strains and two *E. coli* strains is indicated by a log fitting (dashed line) with a fitting goodness of $R^2 = 0.91$. The iron reduction rate was derived by taking the slope of the linear portion of the Fe(III) citrate reduction curves.

to conventional screening methods, such as fluorescence-activated cell sorting (requiring specific fluorophore targets) and proteomic analysis (invasive and time-consuming), dielectrophoretic screening of cell surface polarizability may unlock a vast repertoire of EET-related biochemical applications. Examples include sorting a library of genetically engineered microbes for optimized MFC performance or iron reduction in the iterative process of directed evolution. In addition to EET, other surface features such as the presence of LPS or ion channels may also correlate with cell envelope polarizability. The structure of LPS has a notable impact on bacterial antibiotic resistance, while ion channels are crucial for regulation of membrane potentials and cell electrical signaling. This method will be useful as guidance for further DEP-based phenotypic analysis of a diverse array of cells and organisms.

MATERIALS AND METHODS

Bacterial strains and growth conditions

G. sulfurreducens strain DL-1 and cytochrome-deletion mutants were cultured from frozen stocks, inoculated into and propagated once into liquid growth medium following the study of Coppi *et al.* (*44*). The growth medium was supplemented with 10 mM acetate and 40 mM fumarate as the electron donor and acceptor, respectively, and Wolf's vitamin and mineral supplement [American Type Culture Collection (ATCC)]. The medium (final pH = 6.8) was degassed for 30 min/liter at 80°C in the anaerobic chamber and transferred to glass pressure tubes with butyl stoppers unless otherwise noted. *S. oneidensis* strain MR-1 and mutants were inoculated from frozen stocks and grown in LB broth aerobically at 30°C, 200-rpm shaking for 16 hours, and then transferred 1:100 and grown anaerobically at 30°C for ca. 10 hours in 20 ml of *Shewanella* basal medium (*10*) supplemented with 100 mM HEPES, 0.2% casamino acids, Wolf's vitamin, and a mineral supplement (ATCC). The anaerobic growth medium (final pH = 7.0) also contained either 10 mM lactate and 60 mM fumarate or 20 mM lactate and 15 mM Fe(III) citrate supplemented with 10 mM fumarate. Kanamycin was also provided at a concentration of 50 μM/ml for the growth of ΔMtr complementary mutants (ΔMtr + MtrABC, ΔMtr + MtrDEF, and ΔMtr + vector). *E. coli* strains ccm and ccm + CymA/MtrABC were cultured from frozen stocks and grown aerobically overnight in 2xYT medium at

37°C, 250-rpm shaking, and then transferred 1:100 into 25 ml of 2xYT medium and grown with 250-rpm shaking for 16 hours at 30°C. Then, each strain was centrifuged at 6000 rpm for 4 min and resuspended (with an OD_{600} ~ 0.7) in 20 ml of the anaerobic M1 medium (*42*) supplemented with 0.2% casamino acids, 40 mM lactate, 15 mM Fe(III) citrate, and 10 mM fumarate and grown for 5 days at 30°C. The growth medium also contains kanamycin (50 μM/ml) and chloramphenicol (30 μM/ml). Anaerobic culturing, growth media, and transfers were conducted in an anaerobic chamber (Coy Laboratory Products) with a H_2:CO_2:N_2 (5:20:75) atmosphere.

MFC experimentation

G. sulfurreducens strain DL-1 was cultivated in the anode of an MFC with graphite block electrodes. An H-cell (Adams & Chittenden Scientific Glass) was used as the reactor. The volume of each chamber of the H-cell is 100 ml. A Nafion N117 membrane (Chemours) was boiled in deionized (DI) water and then inserted between the two chambers. A 100-ml DL-1 cell culture was grown to mid-log phase with fumarate, centrifuged, and used to inoculate the anode chamber. To obtain the MFC strain well adapted for reducing insoluble electron acceptors (fig. S2), DL-1 cells were maintained on the growth medium amended with 100 to 120 mM poorly crystalline Fe(III) oxide as the electron acceptor and then transferred (10% inoculum) three times in medium containing 40 mM fumarate before inoculation into the MFC (*4*). The anode chamber contained 100 ml of the growth medium without fumarate. The cathode contained 100 ml of the growth medium lacking fumarate or acetate but included 50 mM potassium ferricyanide as the electron acceptor. The graphite block electrodes were connected by a titanium wire through a 1-kilohm resistor. Current and open circuit voltages of the MFC were monitored periodically using an EX430 MultiMeter (Extech Instruments). The bacterial cells were harvested from the anode (with a 16.6 cm^2 surface area) inside the anaerobic chamber when the MFC approached a current density higher than 45 mA/m^2. The cells were scrapped off the anode surface using a cell scraper (Thermo Fisher Scientific) and suspended in 1.5 ml of their native growth medium.

Iron reduction

The Fe(II) concentration was determined with ferrozine assay adapted from Stookey (*45*). Anaerobic cultures of *S. oneidensis* and *E. coli* strains were grown with Fe(III) citrate and fumarate, identical to the growth condition for the DEP-based screening as mentioned in the previous section. At each time point, one aliquot of each culture was centrifuged at 10,000 rpm for 5 min in the anaerobic chamber to pellet the cells, and 100 μl of the supernatant was acid-extracted in 900 μl of 0.5 M hydrochloric acid (HCl) to yield concentrations within the range of standard curves. The total iron concentration was determined by a separate acid extraction with 10% hydroxylamine hydrochloride in 0.5 M HCl for 24 hours. A hundred microliter of each acid-extracted sample was mixed with 900 μl of ferrozine reagent, which absorbs at 562 nm when chelating Fe(II). The ferrozine reagent contained 10 mM ferrozine (Sigma-Aldrich) in 500 mM HEPES (final pH = 7.0 adjusted by 2N NaOH). The absorbance of all samples was recorded at 562 nm with a UV Vis spectrophotometer (SHIMADZU, Japan) and was used to determine the formation of Fe(II) over time. The Fe(II) concentration in each culture was subtracted by abiotic iron reduction observed in medium-only controls at each time point. Standard curves were made from ferrous sulfate dissolved in 0.5 N HCl.

Sample preparation for 3DiDEP

Bacteria cells reaching stationary phase were fluorescently labeled using 20 μM SYTO BC Green Fluorescent Nucleic Acid Stain (Thermo Fisher Scientific) in their native medium and then centrifuged at 4000 rpm for 4 min. The cells were rinsed once and well mixed using a vortex mixer in their native growth medium to remove the dye before being centrifuged again. The cells were lastly suspended in the DEP buffer that had been left to degas in the anaerobic chamber for 4 weeks. The DEP buffer solution (final pH = 6.8) was prepared by adding DI water to 1× phosphate-buffered saline until the solution conductivity was nearly 100 μS/cm. The DEP buffer also contains 1 to 2% (v/v) glycerol for an osmolarity matching that of the growth medium.

3DiDEP immobilization

Cells were resuspended in the DEP buffer at an OD_{600} of ca. 0.05 and quickly introduced into the 3DiDEP microchannel via the fluidic reservoirs (see section S2 for details about the 3DiDEP microdevice). A "linear sweep" DC voltage difference increasing linearly with time at 1 V/s from 0 to 100 V was applied across the channel via an HVS-448 high-voltage power supply (LabSmith), controlled by a customized LabVIEW program. The SYTO BC fluorescence intensity increased with time as bacterial cells accumulated near the constricted region (movie S1) and was recorded by time-lapse image sequences captured at 1 frame/s using a CoolSNAP HQ2 cooled charge-coupled device (CCD) camera (Photometrics) fitted to an inverted fluorescence microscope (Nikon). The fluorescent intensity data (background subtracted) near the constriction versus time (i.e., the applied voltage) were fitted into a polyline with two segments, whose intersection point was taken as a variable optimized using the least squares method by a customized MATLAB R2015b (MathWorks) code. The applied voltage corresponding to the determined intersection point of the two segments was extracted as the trapping voltage (Fig. 1E) during 3DiDEP.

Linear electrokinetic mobility

The combined linear electrokinetic mobility (μ_{EK}) of each bacterial strain was determined by particle image velocimetry using a PIVlab MATLAB program described previously (*38*). Bacterial motion was tracked in a straight poly(methyl methacrylate) microfluidic channel with the linear sweep DC voltage applied (movie S2). Time lapse image sequences were recorded using a CCD camera, and the PIV program was used to yield the velocity field in the straight microfluidic channel in response to the varying applied voltage. The average velocity versus applied electric field was fitted linearly with the least squares method, and the best-fit slope was taken as the linear electrokinetic mobility for each bacterial strain.

Cell dimensions

After the linear electrokinetic mobility measurement, 10 μl of cell suspension was dropped on a glass slide immediately, air-dried, and observed under a high-magnification optical microscope. Cells for each bacterial strain were fitted into ellipsoids, and their major and minor semi-axes (*a* and *b*) were measured using imageJ (Fig. 2, C to E).

Cell surface polarizability

Numerical simulation was carried out using COMSOL 5.1 Multiphysics Software (COMSOL) to evaluate the local electric field intensity and gradient with prescribed electric potential boundary condition corresponding to the measured trapping voltage for each experiment. The resulting electric field distribution, $\vec{E}$, and gradient of electric

field squared, $\nabla\vec{E}^2$, were averaged over the edges of the microchannel constriction (where DEP reaches the maximum). Along with the linear electrokinetic mobility data, the DEP mobility, μ_{DEP}, for each bacterial strain was extracted using Eq. 7. Substituting the DEP mobility data and cell dimensions into Eq. 6 leads to the Clausius-Mossotti factor, κ_{CM}.

SUPPLEMENTARY MATERIALS

Supplementary material for this article is available at http://advances.sciencemag.org/cgi/content/full/5/1/eaat5664/DC1

Fig. S1. The effect of cell shape on the Clausius-Mossotti factor.
Fig. S2. MFC incubation time affects *G. sulfurreducens* polarizability.
Fig. S3. *S. oneidensis* electrokinetics and cell morphology.
Fig. S4. Electrogenic *E. coli* electrokinetics and cell morphology.
Table S1. Summary of *G. sulfurreducens c*-type outer-membrane cytochromes in this study and their roles in EET.
Movie S1. 3DiDEP immobilization of *G. sulfurreducens*.
Movie S2. Measurement of linear electrokinetic mobility using particle image velocimetry.
Section S1. Calculation of the Clausius-Mossotti factor for two-shelled ellipsoidal particles
Section S2. Microfluidic 3DiDEP device
References (*46*–*48*)

REFERENCES AND NOTES

1. M. E. Hernandez, D. K. Newman, Extracellular electron transfer. *Cell. Mol. Life Sci.* **58**, 1562–1571 (2001).
2. J. K. Fredrickson, M. F. Romine, A. S. Beliaev, J. M. Auchtung, M. E. Driscoll, T. S. Gardner, K. H. Nealson, A. L. Osterman, G. Pinchuk, J. L. Reed, D. A. Rodionov, J. L. M. Rodrigues, D. A. Saffarini, M. H. Serres, A. M. Spormann, I. B. Zhulin, J. M. Tiedje, Towards environmental systems biology of *Shewanella*. *Nat. Rev. Microbiol.* **6**, 592–603 (2008).
3. B. E. Logan, Exoelectrogenic bacteria that power microbial fuel cells. *Nat. Rev. Microbiol.* **7**, 375–381 (2009).
4. D. R. Bond, D. R. Lovley, Electricity production by *Geobacter sulfurreducens* attached to electrodes. *Appl. Environ. Microbiol.* **69**, 1548–1555 (2003).
5. K. Rabaey, R. A. Rozendal, Microbial electrosynthesis—Revisiting the electrical route for microbial production. *Nat. Rev. Microbiol.* **8**, 706–716 (2010).
6. J. S. Deutzmann, M. Sahin, A. M. Spormann, Extracellular enzymes facilitate electron uptake in biocorrosion and bioelectrosynthesis. *MBio* **6**, e00496-15 (2015).
7. K. Inoue, X. Qian, L. Morgado, B.-C. Kim, T. Mester, M. Izallalen, C. A. Salgueiro, D. R. Lovley, Purification and characterization of OmcZ, an outer-surface, octaheme *c*-type cytochrome essential for optimal current production by *Geobacter sulfurreducens*. *Appl. Environ. Microbiol.* **76**, 3999–4007 (2010).
8. C. Leang, M. V. Coppi, D. R. Lovley, OmcB, a *c*-type polyheme cytochrome, involved in Fe(III) reduction in *Geobacter sulfurreducens*. *J. Bacteriol.* **185**, 2096–2103 (2003).
9. T. Mehta, M. V. Coppi, S. E. Childers, D. R. Lovley, Outer membrane *c*-type cytochromes required for Fe(III) and Mn(IV) oxide reduction in *Geobacter sulfurreducens*. *Appl. Environ. Microbiol.* **71**, 8634–8641 (2005).
10. D. Coursolle, J. A. Gralnick, Reconstruction of extracellular respiratory pathways for iron(III) reduction in *Shewanella oneidensis* strain MR-1. *Front. Microbiol.* **3**, 56 (2012).
11. G. Reguera, K. D. McCarthy, T. Mehta, J. S. Nicoll, M. T. Tuominen, D. R. Lovley, Extracellular electron transfer via microbial nanowires. *Nature* **435**, 1098–1101 (2005).
12. S. Pirbadian, S. E. Barchinger, K. M. Leung, H. S. Byun, Y. Jangir, R. A. Bouhenni, S. B. Reed, M. F. Romine, D. A. Saffarini, L. Shi, Y. A. Gorby, J. H. Golbeck, M. Y. El-Naggar, *Shewanella oneidensis* MR-1 nanowires are outer membrane and periplasmic extensions of the extracellular electron transport components. *Proc. Natl. Acad. Sci. U.S.A.* **111**, 12883–12888 (2014).
13. B. A. Methé, K. E. Nelson, J. A. Eisen, I. T. Paulsen, W. Nelson, J. F. Heidelberg, D. Wu, M. Wu, N. Ward, M. J. Beanan, R. J. Dodson, R. Madupu, L. M. Brinkac, S. C. Daugherty, R. T. DeBoy, A. S. Durkin, M. Gwinn, J. F. Kolonay, S. A. Sullivan, D. H. Haft, J. Selengut, T. M. Davidsen, N. Zafar, O. White, B. Tran, C. Romero, H. A. Forberger, J. Weidman, H. Khouri, T. V. Feldblyum, T. R. Utterback, S. E. Van Aken, D. R. Lovley, C. M. Fraser, Genome of *Geobacter sulfurreducens*: Metal reduction in subsurface environments. *Science* **302**, 1967–1969 (2003).
14. C. Leang, L. A. Adams, K.-J. Chin, K. P. Nevin, B. A. Methé, J. Webster, M. L. Sharma, D. R. Lovley, Adaptation to disruption of the electron transfer pathway for Fe(III) reduction in *Geobacter sulfurreducens*. *J. Bacteriol.* **187**, 5918–5926 (2005).
15. X. Qian, G. Reguera, T. Mester, D. R. Lovley, Evidence that OmcB and OmpB of *Geobacter sulfurreducens* are outer membrane surface proteins. *FEMS Microbiol. Lett.* **277**, 21–27 (2007).
16. K. P. Nevin, B.-C. Kim, R. H. Glaven, J. P. Johnson, T. L. Woodard, B. A. Methé, R. J. DiDonato Jr., S. F. Covalla, A. E. Franks, A. Liu, D. R. Lovley, Anode biofilm transcriptomics reveals outer surface components essential for high density current production in *Geobacter sulfurreducens* Fuel Cells. *PLOS ONE* **4**, e5628 (2009).
17. H. Richter, K. P. Nevin, H. Jia, D. A. Lowy, D. R. Lovley, L. M. Tender, Cyclic voltammetry of biofilms of wild type and mutant *Geobacter sulfurreducens* on fuel cell anodes indicates possible roles of OmcB, OmcZ, Type IV pili, and protons in extracellular electron transfer. *Energy Environ. Sci.* **2**, 506–516 (2009).
18. H. Yi, K. P. Nevin, B.-C. Kim, A. E. Franks, A. Klimes, L. M. Tender, D. R. Lovley, Selection of a variant of *Geobacter sulfurreducens* with enhanced capacity for current production in microbial fuel cells. *Biosens. Bioelectron.* **24**, 3498–3503 (2009).
19. R. Y. Adhikari, N. S. Malvankar, M. T. Tuominen, D. R. Lovley, Conductivity of individual *Geobacter* pili. *RSC Adv.* **6**, 8354–8357 (2016).
20. N. S. Malvankar, M. Vargas, K. P. Nevin, A. E. Franks, C. Leang, B.-C. Kim, K. Inoue, T. Mester, S. F. Covalla, J. P. Johnson, V. M. Rotello, M. T. Tuominen, D. R. Lovley, Tunable metallic-like conductivity in microbial nanowire networks. *Nat. Nanotechnol.* **6**, 573–579 (2011).
21. H. Phan, M. D. Yates, N. D. Kirchhofer, G. C. Bazan, L. M. Tender, T.-Q. Nguyen, Biofilm as a redox conductor: A systematic study of the moisture and temperature dependence of its electrical properties. *Phys. Chem. Chem. Phys.* **18**, 17815–17821 (2016).
22. Y. Zhao, D. Chen, Y. Luo, H. Li, B. Deng, S.-B. Huang, T.-K. Chiu, M.-H. Wu, R. Long, H. Hu, X. Zhao, W. Yue, J. Wang, J. Chen, A microfluidic system for cell type classification based on cellular size-independent electrical properties. *Lab Chip* **13**, 2272–2277 (2013).
23. S.-I. Han, Y.-D. Joo, K.-H. Han, An electrorotation technique for measuring the dielectric properties of cells with simultaneous use of negative quadrupolar dielectrophoresis and electrorotation. *Analyst* **138**, 1529–1537 (2013).
24. P. V. Jones, S. Huey, P. Davis, R. McLemore, A. McLaren, M. A. Hayes, Biophysical separation of *Staphylococcus epidermidis* strains based on antibiotic resistance. *Analyst* **140**, 5152–5161 (2015).
25. H. A. Pohl, *Dielectrophoresis: The Behavior of Neutral Matter in Nonuniform Electric Fields* (Cambridge Univ. Press, 1978), p. xii, 579 pp.
26. B. G. Hawkins, C. Huang, S. Arasanipalai, B. J. Kirby, Automated dielectrophoretic characterization of *Mycobacterium smegmatis*. *Anal. Chem.* **83**, 3507–3515 (2011).
27. W. A. Braff, A. Pignier, C. R. Buie, High sensitivity three-dimensional insulator-based dielectrophoresis. *Lab Chip* **12**, 1327–1331 (2012).
28. W. A. Braff, D. Willner, P. Hugenholtz, K. Rabaey, C. R. Buie, Dielectrophoresis-based discrimination of bacteria at the strain level based on their surface properties. *PLOS ONE* **8**, e76751 (2013).
29. M. Castellarnau, A. Errachid, C. Madrid, A. Juárez, J. Samitier, Dielectrophoresis as a tool to characterize and differentiate isogenic mutants of *Escherichia coli*. *Biophys. J.* **91**, 3937–3945 (2006).
30. B. H. Lapizco-Encinas, B. A. Simmons, E. B. Cummings, Y. Fintschenko, Insulator-based dielectrophoresis for the selective concentration and separation of live bacteria in water. *Electrophoresis* **25**, 1695–1704 (2004).
31. K. Khoshmanesh, S. Baratchi, F. J. Tovar-Lopez, S. Nahavandi, D. Wlodkowic, A. Mitchell, K. Kalantar-zadeh, On-chip separation of *Lactobacillus* bacteria from yeasts using dielectrophoresis. *Microfluid. Nanofluid.* **12**, 597–606 (2012).
32. R. Rusconi, J. S. Guasto, R. Stocker, Bacterial transport suppressed by fluid shear. *Nat. Phys.* **10**, 212–217 (2014).
33. R. D. Miller, T. B. Jones, Electro-orientation of ellipsoidal erythrocytes. Theory and experiment. *Biophys. J.* **64**, 1588–1595 (1993).
34. F. Perrin, Mouvement Brownien d'un ellipsoide (II). Rotation libre et dépolarisation des fluorescences. Translation et diffusion de molécules ellipsoidales. *J. Phys. Radium* **7**, 1–11 (1936).
35. T. B. Jones, *Electromechanics of Particles* (Cambridge Univ. Press, 2005), p. xxii, 265 pp.
36. J. Ding, R. M. Lawrence, P. V. Jones, B. G. Hogue, M. A. Hayes, Concentration of Sindbis virus with optimized gradient insulator-based dielectrophoresis. *Analyst* **141**, 1997–2008 (2016).
37. J. W. Voordeckers, B.-C. Kim, M. Izallalen, D. R. Lovley, Role of *Geobacter sulfurreducens* outer surface *c*-type cytochromes in reduction of soil humic acid and anthraquinone-2,6-disulfonate. *Appl. Environ. Microbiol.* **76**, 2371–2375 (2010).
38. Q. Wang, N. N. Dingari, C. R. Buie, Nonlinear electrokinetic effects in insulator-based dielectrophoretic systems. *Electrophoresis* **38**, 2576–2586 (2017).
39. N. N. Dingari, C. R. Buie, Theoretical investigation of bacteria polarizability under direct current electric fields. *Langmuir* **30**, 4375–4384 (2014).
40. S. M. Strycharz, A. P. Malanoski, R. M. Snider, H. Yi, D. R. Lovley, L. M. Tender, Application of cyclic voltammetry to investigate enhanced catalytic current generation by biofilm-modified anodes of *Geobacter sulfurreducens* strain DL1 vs. variant strain KN400. *Energy Environ. Sci.* **4**, 896–913 (2011).
41. G. F. White, Z. Shi, L. Shi, Z. Wang, A. C. Dohnalkova, M. J. Marshall, J. K. Fredrickson, J. M. Zachara, J. N. Butt, D. J. Richardson, T. A. Clarke, Rapid electron exchange between surface-exposed bacterial cytochromes and Fe(III) minerals. *Proc. Natl. Acad. Sci. U.S.A.* **110**, 6346–6351 (2013).

42. H. M. Jensen, M. A. TerAvest, M. G. Kokish, C. M. Ajo-Franklin, CymA and exogenous flavins improve extracellular electron transfer and couple it to cell growth in Mtr-expressing *Escherichia coli*. *ACS Synth. Biol.* **5**, 679–688 (2016).
43. S. H. Light, L. Su, R. Rivera-Lugo, J. A. Cornejo, A. Louie, A. T. Iavarone, C. M. Ajo-Franklin, D. A. Portnoy, A flavin-based extracellular electron transfer mechanism in diverse Gram-positive bacteria. *Nature* **562**, 140–144 (2018).
44. M. V. Coppi, C. Leang, S. J. Sandler, D. R. Lovley, Development of a genetic system for *Geobacter sulfurreducens*. *Appl. Environ. Microbiol.* **67**, 3180–3187 (2001).
45. L. L. Stookey, Ferrozine—A new spectrophotometric reagent for iron. *Anal. Chem.* **42**, 779–781 (1970).
46. R. Hölzel, Non-invasive determination of bacterial single cell properties by electrorotation. *BBA-Mol. Cell. Res.* **1450**, 53–60 (1999).
47. T. J. Silhavy, D. Kahne, S. Walker, The bacterial cell envelope. *Cold Spring Harb. Perspect. Biol.* **2**, a000414 (2010).
48. W. Vollmer, S. J. Seligman, Architecture of peptidoglycan: More data and more models. *Trends Microbiol.* **18**, 59–66 (2010).

Acknowledgments: We thank D. R. Lovley and C. M. Ajo-Franklin for supplying *G. sulfurreducens* and *E. coli* strains studied in this work. We acknowledge N. Fuller for creation of aspects of Fig. 1D. **Funding:** This work was partially supported by the NSF (award number 1150615) and the Institute for Collaborative Biotechnologies through grant W911NF-09-0001 from the U.S. Army Research Office. The content of the information does not necessarily reflect the position or the policy of the government, and no official endorsement should be inferred.
Author contributions: Q.W., A.-A.D.J., and C.R.B. designed the experiments. L.L. and C.R.B. planned the project. J.A.G. provided the *S. oneidensis* strains and guided the cell cultivation. Q.W. cultured *S. oneidensis* and *E. coli* strains, fabricated the microfluidic devices, carried out the experiments and COMSOL simulation, and calculated the data. A.-A.D.J. cultured *G. sulfurreducens* strains and operated the MFCs. All authors co-analyzed the data and wrote the paper. **Competing interests:** The authors declare that they have no competing interests. **Data and materials availability:** All data needed to evaluate the conclusions in the paper are present in the paper and/or the Supplementary Materials. Additional data related to this paper may be requested from the authors.

Submitted 12 March 2018
Accepted 30 November 2018
Published 11 January 2019
10.1126/sciadv.aat5664

Citation: Q. Wang, A.-A. D. Jones III, J. A. Gralnick, L. Lin, C. R. Buie, Microfluidic dielectrophoresis illuminates the relationship between microbial cell envelope polarizability and electrochemical activity. *Sci. Adv.* **5**, eaat5664 (2019).

Science Advances

Microfluidic dielectrophoresis illuminates the relationship between microbial cell envelope polarizability and electrochemical activity

Qianru Wang, A.-Andrew D. Jones III, Jeffrey A. Gralnick, Liwei Lin and Cullen R. Buie

Sci Adv **5** (1), eaat5664.
DOI: 10.1126/sciadv.aat5664